IEICE TRANS. COMMUN., VOL.E88–B, NO.2 FEBRUARY 2005

PAPER

A Frequency Scheduling Method for MC-CDM

Shigehiko TSUMURA[†a)], ***Student Member***, **Yoshitaka HARA**[††], ***and*** **Shinsuke HARA**[†], ***Members***

SUMMARY Multi-carrier code division multiplexing (MC-CDM) is one of promising multiplexing techniques for fourth-generation mobile downlink communications systems, where high data rate services should be provided even for high speed-cruising mobiles. For MC-CDM-based packet communication, a frequency scheduling method, which adaptively assigns different sub-carriers to different users, is proposed. This paper proposes a frequency scheduling method, which utilizes pre-assignmented subcarriers in the frequency domain for the MC-CDM scheme. Furthermore, the performance of the proposed system in frequency selective fading channels is compared with that of a no-scheduled MC-CDM scheme by computer simulation in both single- and multi-cell environments. From the results, it is found that the proposed system achieves better bit error rate performance than the no-scheduled MC-CDM scheme and can control quality of service (QoS) for active users.

key words: *frequency selective fading channel, multi-carrier code division multiplexing (MC-CDM), multi-user channel, resource management*

1. Introduction

Multi-carrier code division multiplexing (MC-CDM), which is a combination of orthogonal frequency division multiplexing (OFDM) and CDM, has been drawing much attention as a promising downlink protocol for next generation mobile communications systems, where high-speed data transmission is required [1], [2]. This is because multicarrier communication makes fading over subcarriers frequency-non-selective, namely, the bandwidth of each subcarrier is narrow enough in comparison to the coherent bandwidth of the channel, and insertion of guard interval (GI) mitigates inter-symbol-interference (ISI) caused by delay spread. Moreover, MC-CDM receiver can effectively combine all the received signal energy scattered in the frequency domain, on the other hand, it could be difficult for a rake receiver of direct sequence (DS)-CDM scheme to combine all the received signal energy scattered in the time domain. That is to say, as the number of resolvable paths increases, the complexity of the rake receivers increases and the inter-path interference among a lot of paths degrades the performance of the DS-CDM system. Consequently, it has been reported that the MC-CDM downlink system has superiority over the DS-CDM system [3]–[5].

On the other hand, the benefits of link adaptation, which modifies the transmission parameters in accordance with the channel conditions for mobile users, are well known. For instance, high-speed downlink packet access (HSDPA) based on WCDMA air interface contains such link adaptation techniques as adaptive modulation and coding schemes, hybrid automatic repeat request, and fast scheduling [6]. Here, for the scheduler, data are transmitted to different users in a time division multiplexing manner, so as to increase the system capacity [7].

Moreover, for multicarrier transmission systems, scheduling algorithms which adaptively assign channels not only in the time domain but also in the frequency domain have been proposed [8]–[14]. They are mainly categorized into two groups, namely, one is OFDM-based scheduling algorithms [8]–[11] whereas the other is MC-CDM-based scheduling algorithms [12]–[14]. CDM technique has a one more freedom in the code domain, so it is expected that the MC-CDM-based scheduling algorithms can have a more flexibility in channel assignment, as compared with the OFDM-based scheduling algorithms. In [12], [13], a base station adaptively assigns a packet to each user with multiple blocks of subcarriers multiplexed by spreading codes, where interfering signal is assumed as a white noise. Assignment with a single block of subcarriers can make the scheduling algorithm be much simpler.

This paper proposes a simple frequency scheduling algorithm for MC-CDM. As in [14], the proposed algorithm adaptively allocates a single block of subcarriers (called "*segment* " in this paper) with the highest signal to interference plus noise power ratio (SINR) is adaptively allocated for each user (see Fig. 1), and contains a novel calculation method of inter-cell interference power suited for practical multi-cell environments.

The remainder of this paper is organized as follows. We first describe the transmitter and the receiver for the pro-

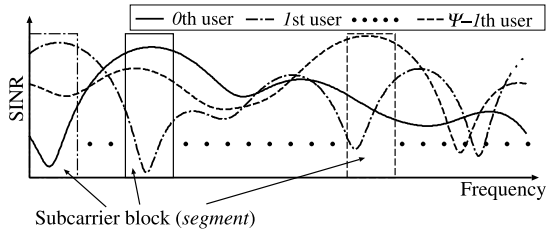

Fig. 1 Basic idea of frequency scheduling.

Manuscript received July 7, 2004.
Manuscript revised October 12, 2004.

[†]The authors are with the Department of Electronic, Information Systems and Energy Engineering, Graduate School of Engineering, Osaka University, Suita-shi, 565-0871 Japan.

[††]The author is with the Mitsubishi Electric Information Technology Centre Europe B.V. (ITE), 1, allee de Beaulieu, CS 10806, 35708 Rennes Cedex 7, France.

a) E-mail: tsumura@eie.eng.osaka-u.ac.jp

posed system in Sect. 2. Next, Sect. 3 proposes the algorithm for the frequency scheduling. In Sect. 4, we then discuss the performance of the MC-CDM with the frequency scheduling in both single- and multi-cell environments. Finally, Sect. 5 presents the concluding remarks.

2. System Model

2.1 Transmitter

In Fig. 2, the block diagram of a base station for the MC-CDM scheme with the proposed frequency scheduling, which can handle data sequences for total Ψ users. The binary information sequence of the ψth ($\psi = 0, \cdots, \Psi - 1$) user is first turbo encoded and then quadrature phase shift keying (QPSK)-modulated. The turbo encoder is formed by parallel concatenation of two RSC encoders separated by a pseudo-random interleaver [15]. The first RSC encodes directly the input sequence and has two outputs. The first output is equal to the input sequence since the encoder is systematic and the other output is a parity check sequence. Note that the first RSC encoder is forced to the all-zero state at the end of the input sequence. The interleaved information sequence is fed to the second RSC encoder. For the turbo code with rate of $1/2$, the parity check digits from the two RSC encoders are alternately deleted. The punctured output of the turbo code at a time instant consists of an information digit followed by a parity check digit which is alternately obtained from the first and the second RSC encoders. The QPSK modulated symbols with the symbol rate

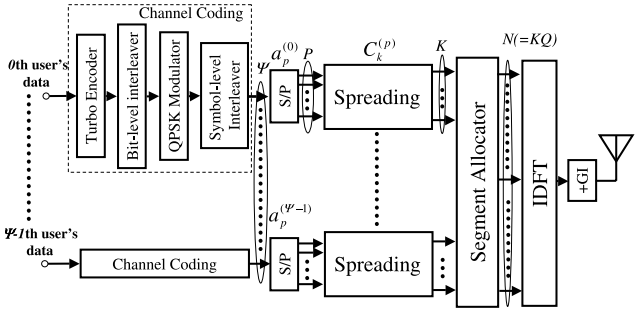

Fig. 2 Transmitter structure.

of R for the ψth user in the ith ($= 0, \cdots, I-1$) transmit packet where I is the number of MC-CDM symbols in one packet, are first converted into P parallel sequences $\{a_1^{(\psi)}(i), \cdots, a_{P-1}^{(\psi)}(i)\}, a_p^{(\psi)}(p = 0, \cdots, P-1) \in \{\pm 1/\sqrt{2} \pm j/\sqrt{2}\}$, and then each parallel sequence is multiplied with an orthogonal short code with length of K and a cell-specific long scrambling code which is common to the segment in a given cell in the downlink. We employ a pseudo noise (PN) sequence of length $2^{15} - 1$ as the scrambling code [16], and shifted PN sequences are used among cells. In the following, for simplicity, we omit the multiplication of the long code and regard the long code effects as being included in the spreading code $c_k^{(p)}(k = 0, 1, \cdots, K-1) \in \{\pm 1/\sqrt{K}\}$. With the segment allocator, the spread symbols of the ψth user is allocated to the $q_\psi(q_\psi = 0, 1, \cdots, Q-1)$th segment (see Fig. 3 as an example of the segment configuration for $q_\psi = \psi$ and $Q = \Psi$), according to the SINR information of the segments for all the active users. Here, the segment, where the data of the user are multiplexed by the spreading code, consists of K adjacent subcarriers instead of interleaved subcarriers, since the reduction of inter-code interference (ICI) due to multi-path fading is required for the proposed system. That is, the blocked-spreading manner can reduce effect of multi-path fading by increasing the fading correlation among the subcarriers [17], [18]. The details of the allocation algorithm will be shown in Sect. 3. With the $N(= K \times Q)$-point inverse discrete Fourier transform (IDFT), the allocated symbols are modulated. The outputs of the IDFT are converted back into a serial sequence and a GI is inserted in each IDFT output. As a result, the GI insertion can avoid ISI caused by multi-path fading. The complex equivalent low-pass transmitted signal $s(t)$ is written as

$$s(t) = \sum_{\psi=0}^{\Psi-1} \sum_{i=0}^{I-1} \sum_{p=0}^{P-1} \sum_{k=0}^{K-1} a_p^{(\psi)}(i) c_k^{(p)} \cdot p_s(t - iT_s) \exp(j2\pi(q_\psi K + k) f'(t - iT_s)), \quad (1)$$

$$T_s = Q/R, \quad (2)$$

$$f' = 1/(T_s - \Delta) = 1/t_s, \quad (3)$$

where f', T_s and t_s denote the minimum subcarrier separation, the MC-CDM symbol duration including GI Δ and the

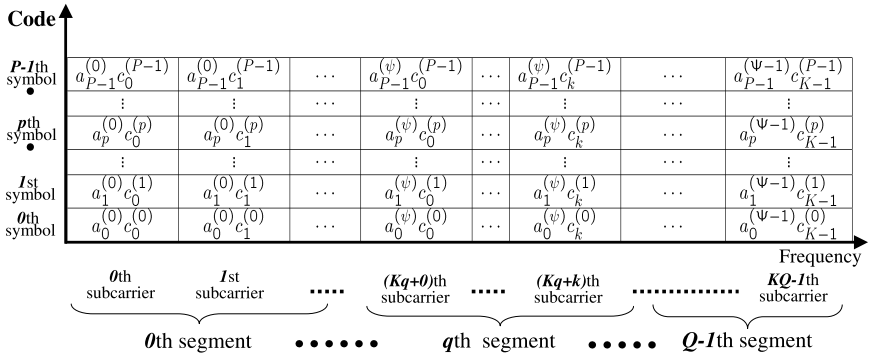

Fig. 3 Segment configuration ($q_\psi = \psi$, $Q = \Psi$).

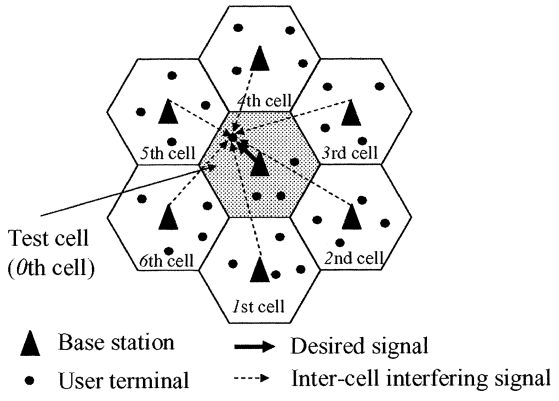

Fig. 4 Multi-cell environment.

symbol duration per subcarrier, respectively, and $p_s(t)$ is the rectangular symbol pulse waveform defined as

$$p_s(t) = \begin{cases} 1 & -\Delta \le t < t_s, \\ 0 & \text{otherwise.} \end{cases} \tag{4}$$

2.2 Channel Model

We assume a multi-cell environment composed of seven cells as shown in Fig. 4. The users are uniformly distributed in each cell, and the number of users in each cell is identical. We evaluate the performance of users in the central cell. The received power of the desired signal and the inter-cell interfering signals follow the path loss with the decay factor of 4 and log-normal shadowing with the standard deviation of 8 dB. The average received power of the desired signal is larger than the total power of the interfering signals. Furthermore, the frequency-selective Rayleigh fading channel is modeled as a wide-sense stationary uncorrelated scattering (WSSUS) channel with L received paths with a complex equivalent low-pass time-variant impulse response:

$$h_m(\tau, t) = \sum_{l=0}^{L-1} g_m^{(l)}(t)\delta(\tau - \tau_m^{(l)}), \tag{5}$$

where $\delta(\cdot)$ and $\tau_m^{(l)}$ denote the Dirac's delta function and the propagation delay for the lth path between the transmit antenna and the mth receive antenna, respectively. $g_m^{(l)}(t)$ is the lth path gain between the transmit antenna and the mth receive antenna, modeled as a mutually independent complex Gaussian random process with zero mean and variance $(\sigma_m^{(l)})^2$ for different l and m. A constraint $E[\sum_{l=0}^{L-1} \sigma_m^{(l)2}] = 1$ is made in the evaluation of the performance in the single cell scenario ($E[\cdot]$ stands for the ensemble mean). We also assume a low mobility 10-path Rayleigh fading channel;

$$(\sigma_m^{(l)})^2 = \exp\left(\frac{-\tau_m^{(l)}}{\tau_{RMS}}\right) \Big/ \sum_{l=0}^{L-1} \exp\left(\frac{-\tau_m^{(l)}}{\tau_{RMS}}\right), \tag{6}$$

where τ_{RMS} denotes the root mean square (RMS) delay spread of the channel model, $L = 10$ and $\tau_m^{(l+1)} - \tau_m^{(l)} = 5t_s/N$. In this model, no ISI occurs for the desired signal, because the maximum delay spread for this model is around 50 samples and the GI for the MC-CDM scheme is 128 samples in the computer simulation.

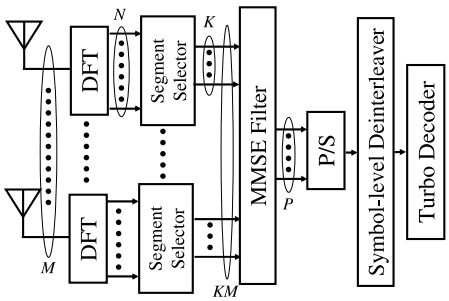

Fig. 5 Receiver structure.

The received signal for the mth receive antenna $x_m(t)$ is given by

$$x_m(t) = \int_{-\infty}^{+\infty} \sum_{f=0}^{6} s_n^{(f)}(t-\tau) h_m^{(f)}(\tau, t) d\tau + \eta_m(t), \tag{7}$$

where f is the cell index and $\eta_m(t)$ denotes a complex Gaussian noise.

2.3 Receiver

Figure 5 shows the receiver structure for the proposed system. For the received signal of each antenna, each subcarrier component is first detected with the discrete Fourier transform (DFT) and the allocated segment of the ψth user is picked up with the segment selector. For simplicity, we consider the received signal of the ψth user for whom the $q_\psi(=0)$th segment is allocated, in the $f(=0)$th cell at the $i(=0)$th MC-CDM symbol. Then, the received subcarrier components at the mth received antenna can be expressed as

$$\boldsymbol{r}_m = \boldsymbol{H}_m \boldsymbol{a} + \boldsymbol{\eta}_m, \tag{8}$$

where the received signal vector $\boldsymbol{r}_m$ ($K \times 1$), the channel matrix $\boldsymbol{H}_m$ ($K \times P$), the ψth user's coded symbol vector $\boldsymbol{a}$ ($P \times 1$) and the noise plus inter-cell interference signals vector $\boldsymbol{\eta}_m$ ($K \times 1$) are given by

$$\begin{aligned} \boldsymbol{r}_m &= [r_0^{(m)}, r_1^{(m)}, \cdots, r_{K-1}^{(m)}]^T \\ \boldsymbol{a} &= [a_0, a_1, \cdots, a_{P-1}]^T, \\ \boldsymbol{\eta}_m &= [\eta_0^{(m)}, \eta_1^{(m)} \cdots, \eta_{K-1}^{(m)}]^T, \end{aligned}$$

where $r_k^{(m)}$ denotes the mth receive antenna's kth received subcarrier component, superscript T stands for transposition, and

$$\boldsymbol{H}_m = \begin{bmatrix} H_m^{(0)}c_0^{(0)} & H_m^{(0)}c_0^{(1)} & \cdots & H_m^{(0)}c_0^{(P-1)} \\ H_m^{(1)}c_1^{(0)} & H_m^{(1)}c_1^{(1)} & \cdots & H_m^{(1)}c_1^{(P-1)} \\ \vdots & \vdots & \ddots & \vdots \\ H_m^{(K-1)}c_{K-1}^{(0)} & H_m^{(K-1)}c_{K-1}^{(1)} & \cdots & H_m^{(K-1)}c_{K-1}^{(P-1)} \end{bmatrix} \tag{9}$$

where $H_m^{(k)}$ denotes the channel response at the mth receive antenna for the kth received subcarrier component. In addition, the received subcarrier components for M receive antennas can be expressed as

$$\boldsymbol{r} = \boldsymbol{H}\boldsymbol{a} + \boldsymbol{\eta}, \tag{10}$$

where

$$\begin{aligned} &\boldsymbol{r} = [\boldsymbol{r}_1^T, \cdots, \boldsymbol{r}_M^T]^T (MK \times 1), \\ &\boldsymbol{H} = [\boldsymbol{H}_1^T, \cdots, \boldsymbol{H}_M^T]^T (MK \times P), \\ &\boldsymbol{\eta} = [\boldsymbol{\eta}_1^T, \cdots, \boldsymbol{\eta}_M^T]^T (MK \times 1). \end{aligned} \tag{11}$$

The minimum mean square (MSE) criterion for the pth transmit symbol of the ψth user symbol is given by

$$\arg\min_{\boldsymbol{w}_p} E\left[\left|a_p - \boldsymbol{w}_p^H \boldsymbol{r}\right|^2\right], \tag{12}$$

where $\boldsymbol{w}_p$ is the weight vector of the MMSE filter and superscript H stands for Hermitian transpose. In the following, we assume that the coded data symbols are independent for different symbols and complex random variables with zero mean and unit variance. It is well known that the weight vector, which minimizes the MSE, is given by the Wiener solution:

$$\boldsymbol{w}_p = \boldsymbol{R}^{-1}\boldsymbol{p}_p \tag{13}$$

where the cross-correlation vector $\boldsymbol{p}_p$ between the received signal and the pth desired symbol is given by

$$\begin{aligned} \boldsymbol{p}_p = [&H_0^{(0)}c_0^{(p)}, H_0^{(1)}c_1^{(p)}, \cdots, H_0^{(K-1)}c_{K-1}^{(p)}, \\ &H_1^{(1)}c_0^{(p)}, \cdots, H_M^{(K-1)}c_{K-1}^{(p)}]^T (MK \times 1) \end{aligned} \tag{14}$$

and the auto-correlation matrix of the received signal $\boldsymbol{R}$ is

$$\boldsymbol{R} = \boldsymbol{H}\boldsymbol{H}^H + \begin{bmatrix} \sigma_0^2 & 0 & \cdots & 0 \\ 0 & \sigma_1^2 & \ddots & 0 \\ \vdots & \ddots & \ddots & 0 \\ 0 & 0 & \cdots & \sigma_{MK-1}^2 \end{bmatrix} \tag{15}$$

where

$$\sigma_i^2 = \sigma_{noise}^2 + N_i^{(q_\psi)} \quad \text{for} \quad i = 0, 1, \cdots MK-1 \tag{16}$$

where σ_{noise}^2 is the variance of the noise and $N_i^{(q_\psi)}$ denotes the average power of the interfering signals from the neighboring cells in the kth subcarrier component for the q_ψth segment at the mth receive antenna. Then, $N_i^{(q_\psi)}$ is given by

$$N_i^{(q_\psi)} = \frac{P}{K}\sum_{\psi'=0}^{\Psi-1}\sum_{f=1}^{6} |H_m^{(k),(f)}|^2 \delta(q_{\psi'}^{(f)} - q_\psi^{(0)}) \quad \text{for} \quad i = mK + k \tag{17}$$

where $q_\psi^{(f)}$ denote the segment number allocated to the ψth user in the fth cell. With the MMSE filter, the decision variable for the pth symbol of the ψth user y_p is given by

$$y_p = \boldsymbol{w}_p^H \boldsymbol{r}. \tag{18}$$

The MMSE filter outputs after the symbol-level deinterleaver are fed into the turbo decoder with two Log-MAP (maximum *a posteriori*) decoders which calculate the bit-level log-likelihood ratio (LLR) for the MMSE filter outputs based on a Gaussian approximation [19], [20].

3. Proposed Frequency Scheduling Algorithm

Figure 6 shows the flowchart of the proposed segment allocation method for the MC-CDM scheme with the frequency scheduling. In the following discussion, we consider the 0th cell.

Step. 1: From SINRs of all active users, the base station sets a table as shown in Fig. 7. With $\zeta = q_\psi K + k$, the SINR of the q_ψth segment γ_{q_ψ} is given by

$$\gamma_{q_\psi} = P\sum_{k=0}^{K-1}\sum_{m=0}^{M-1} \frac{|H_m^{(\zeta)}|^2}{(\sigma_{noise}^2 + N_\zeta'^{(q_\psi)})} \tag{19}$$

where $N_\zeta'^{(q_\psi)}$ is the expected inter-cell interference component in the kth subcarrier component at the mth receive antenna for the q_ψth segment based on the last packet transmission;

$$N_\zeta'^{(q_\psi)} = \frac{P}{K}\sum_{\psi'=0}^{\Psi-1}\sum_{f=1}^{6} |H_m^{(\zeta),(f)}|^2 \delta(q_{\psi'}'^{(f)} - q_\psi) \tag{20}$$

where it is assumed that the $q_\psi'^{(f)}$ is allocated to the ψth user in the fth cell for the last packet transmission.

The reason why we use Eq.(20) for calculation of inter-cell interference power is that the proposed scheduler does not know the SINR information of the other cells. If the SINRs of the other cells are available at its own cell, which may be notified by the other cells, the segment can be optimally assigned so as to maximize the SINRs for all the active users even in the multi-cell environment. However, the scheduling algorithm may become much more complicated. The proposed scheduling algorithm calculates the power of inter-cell interference with Eq.(20) without information from other cells, so it is simple and suited for practical multi-cell environments.

Step. 2: For all the users who are not allocated the transmission segment, we find a candidate of the transmission segment for the ψth user $\tilde{q_\psi}$, which maximizes the SINR among the unallocated segments of the ψth user:

$$\tilde{q_\psi} = \max\{\gamma_{q_\psi}\} \text{ for unallocated segments.} \tag{21}$$

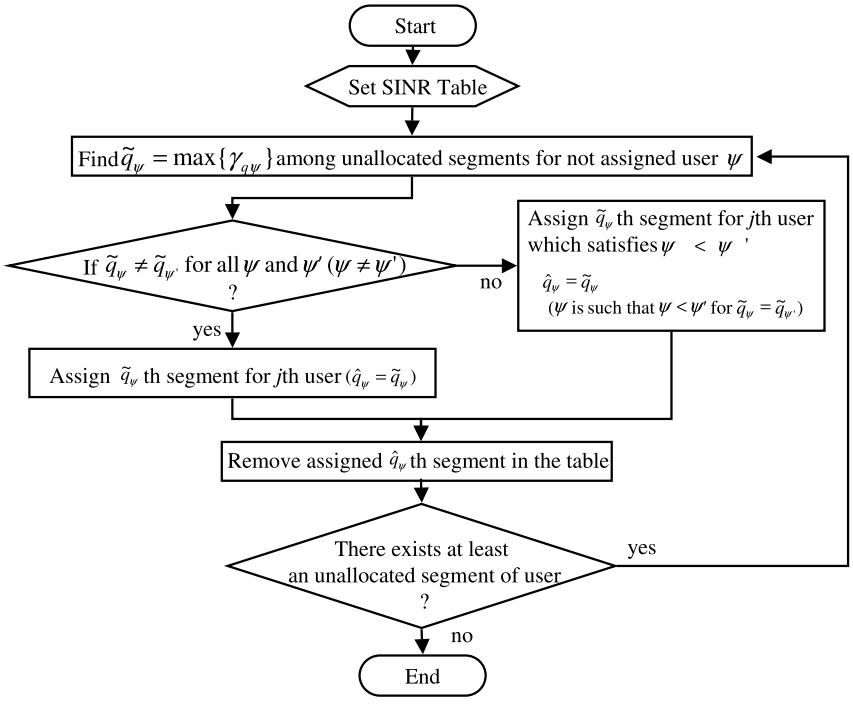

Fig. 6 Flowchart of proposed allocation method.

	0th segment		**q**th segment		**Q-1**th segment
0th user	γ_{0_0}	$\cdots$	γ_{q_0}	$\cdots$	$\gamma_{(Q-1)_0}$
	$\vdots$	$\cdots$	$\vdots$	$\cdots$	$\vdots$
ψth user	γ_{0_ψ}	$\cdots$	γ_{q_ψ}	$\cdots$	$\gamma_{(Q-1)_\psi}$
	$\vdots$	$\cdots$	$\vdots$	$\cdots$	$\vdots$
Ψ-**1**th user	$\gamma_{0_{\Psi-1}}$	$\cdots$	$\gamma_{q_{\Psi-1}}$	$\cdots$	$\gamma_{(Q-1)_{\Psi-1}}$

Fig. 7 Configuration SINR table.

Step. 3: If $\tilde{q_\psi} \neq \tilde{q_{\psi'}}$ for all ψ and ψ' except for $\psi = \psi'$, $\hat{q_\psi}$, which is the segment allocated for the ψth user, is $\tilde{q_\psi}$. Otherwise, $\tilde{q_\psi}$, where ψ is such that $\psi < \psi'$ for $\tilde{q_\psi} = \tilde{q_{\psi'}}$, is selected for $\hat{q_\psi}$

Step. 4: $\gamma_{\hat{q_\psi}}$ is removed from the SINR table. That is, the $\hat{q_\psi}$th segment is eliminated from the candidates for the transmission segment.

Step. 5: If there exists at least an unallocated segment for an active user, return to *Step. 2*. Otherwise, the allocation algorithm is terminated and the data for the ψth user are transmitted with the $\hat{q_\psi}$th segment. Then, the subcarriers corresponding to the unallocated segment are assigned to zero.

In the proposed system, the data of the user are transmitted in the allocated segment where the SINR is larger than the SINR averaged in all the received subcarriers. Therefore, taking into account the fact that the channel of different users is different in the frequency domain, the proposed system can make efficient use of the *"multi-user diversity"* [8] effect as well as the frequency diversity effect, although a no-scheduled MC-CDM scheme only makes use of the frequency diversity effect. Moreover, without the SINR information for the segments in the other cells, the proposed system autonomously and dynamically allocates the segment with higher SINR which is estimated for the last transmission in its own cell. That is, in the case of the multi-cell environment, the performance of the proposed system can be much better than that of a no-scheduling MC-CDM scheme.

Moreover, the transmission delay of the proposed scheduler, which allocates the channel of active users in the frequency domain, is less than that of scheduler in the time domain (e.g. max C/I, round robin and proportional fairness discussed in 3GPP). Also, in the proposed algorithm, QoS for active users can be controlled. The SINR of the allocated segment γ_{q_ψ}, here, becomes gradually greater as the user number index ψ decreases in the proposed algorithm. Therefore, the proposed scheduler selecting user number index ψ makes it possible to control the performance among active users.

4. Computer Simulation

Link-level simulations are conducted to evaluate the performance of the proposed system in both single- and multi-cell environments. For the sake of comparison, we also evaluate the performance of the MC-CDM scheme without the scheduler, where the alignment of the post-spread symbol in the frequency domain $a_p^{(\psi)} c_k^{(\psi)}$ is interleaved by each ϕ subcarriers [21], where ϕ is the number of serial-to-parallel conversions. With the frequency-interleaved spreading, therefore, the MC-CDM scheme without the scheduler makes it

Table 1 System parameters.

Transmission bit rate per user R	2 [Mbits/sec]
Channel encoding	Turbo coding (constrain length of 4, rate of 1/2) RSC generators of (15,17) in octal form
Channel decoding	Log-MAP algorithm (8 iterations)
Symbol-level interleaver	Pseudo-Random Interleaver (size of 1024 symbols)
Bit-level interleaver	Pseudo-Random Interleaver (size of 2048 bits)
Channel model	10-path exponentially decaying model
Packet length I	64
Number of sub-carriers N	512
Code length K	32 (Walsh Hadamard)
Number of segments Q	16
Number of multiplexed symbol per segment P	16
Effective symbol duration t_s	6.4 [μsec]
GI Δ	1.6 [μsec]
Number of receive antennas M	2

possible to obtain frequency diversity effects in frequency selective fading channels.

Table 1 shows the parameters in the computer simulation. For fair comparison, the radio link parameters of the MC-CDM scheme with the proposed scheduler are set based on the conventional MC-CDM scheme [2]. The transmission information data rate per user of 2[Mbits/sec], after a turbo coding (rate of 1/2 and constrain length of 4) and QPSK modulation, the number of sub-carriers N of 512, spreading code length K of 32, the number of serial-to-parallel conversions ϕ of 16, the bandwidth of 80[MHz] and the number of MC-CDM symbols in one packet I of 64 are given for the link parameters. The number of segments Q and number of multiplexed symbols per segment P become 16 and 16, respectively, for the given parameters. Also, the effective symbol duration and the GI duration become 6.4 [μsec] and 1.6 [μsec], respectively. For the proposed scheduling algorithm, it is also assumed that estimation of the SINR of the segments can be perfect and the user successfully knows the segment allocated in the base station.

In the following figures, with the two receive antennas ($M = 2$), we discuss the performance for the MC-CDM scheme with the proposed scheduler and the conventional MC-CDM scheme. Then, we define $\overline{E_s/N_0}$ as the average signal to noise power spectrum density ratio per QPSK symbol of user per receive antenna.

4.1 Single-Cell Environment

In this subsection, the performance of the MC-CDM scheme with and without the proposed scheduler is evaluated in the single-cell environment.

Figure 8 shows the coded bit error rate (BER) performance with the turbo coding for the MC-CDM scheme with and without the proposed frequency scheduling in the single-cell environment where the RMS delay spread is 200 [nsec]. Furthermore, with the proposed scheduler, Fig. 9 shows the coded BER performance of all the active users and the user for whom the scheduler allocates the segment with the smallest SINR among all the transmission segments in one packet transmission for $\Psi = 8$ and 16. From Fig. 8, we can see that the coded BER performance with the proposed scheduler is better than that without the scheduler for $\Psi = 1$ and 8, while the coded BER performance with the proposed scheduler is worse than that without the scheduler for $\Psi = 16$ in $\overline{E_s/N_0} > 4$ [dB]. Also, the improvement between the proposed system and the no-scheduled MC-CDM scheme in the smaller $\overline{E_b/N_0}$ becomes greater, as the number of active users decreases. From Fig. 9, the allocation of the segment with the lowest SINR among all the allocated segments is considered as a major cause of the coded BER floor for $\Psi = 16$ in the higher $\overline{E_b/N_0}$ region. In other words, the MC-CDM scheme with the proposed scheduler may allocate the transmission segment, whose SINR is lower than that in all the received subcarriers for certain active users, i.e., the probability of the allocation of the segment with lower SINR becomes greater as the number of active users increases.

In order to investigate the frequency diversity effect caused by the channel coding for the MC-CDM scheme with

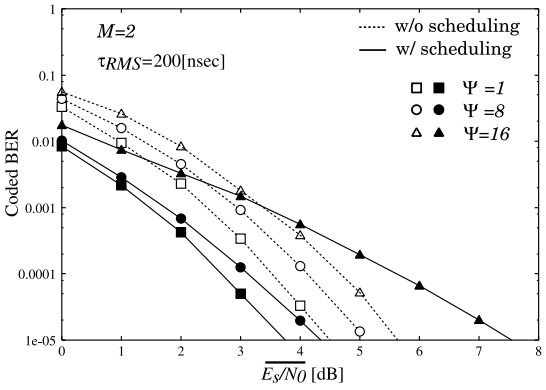

Fig. 8 Coded BER performance with and without frequency scheduling for $\Psi = 1, 8, 16$. ($\tau_{RMS} = 200$ [nsec])

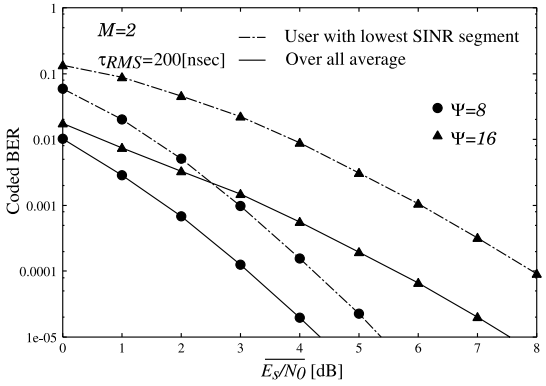

Fig. 9 Coded BER performance with frequency scheduling for $\Psi = 8$ and 16. ($\tau_{RMS} = 200$ [nsec])

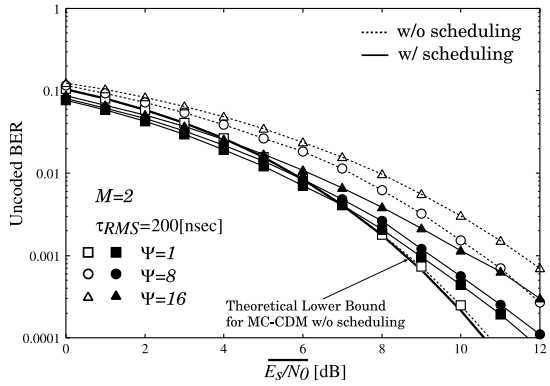

Fig. 10 Uncoded BER performance with and without frequency scheduling $\Psi = 1, 8, 16$. ($\tau_{RMS} = 200$ [nsec])

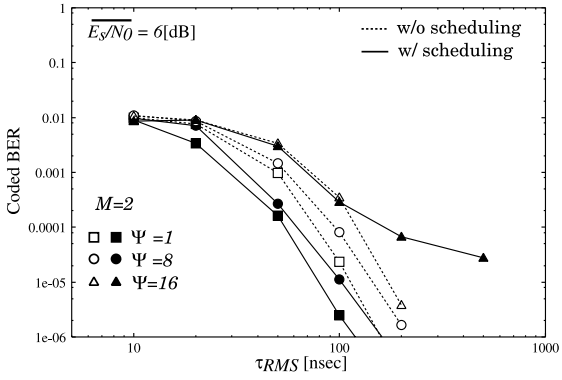

Fig. 11 Coded BER versus τ_{RMS} for $\Psi = 1, 8, 16$. ($\overline{E_s/N_0} = 6$ [dB])

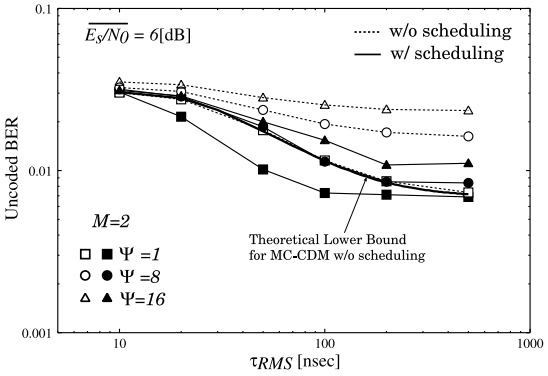

Fig. 12 Uncoded BER versus τ_{RMS} for $\Psi = 1, 8, 16$. ($\overline{E_s/N_0} = 6$ [dB])

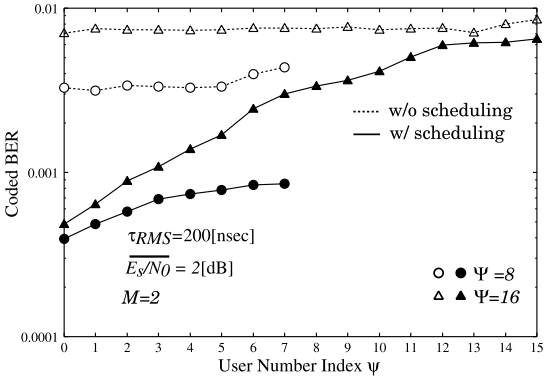

Fig. 13 Coded BER versus user number index ψ for $\Psi = 8$ and 16. (τ_{RMS} =200 [nsec] and $\overline{E_s/N_0}$ =2 [dB])

and without the proposed scheduler, the uncoded BER performance with and without the proposed scheduler for Ψ =1, 8 and 16 is plotted in Fig. 10. For the purpose of reference, the theoretical lower bound of the uncoded BER for the MC-CDM scheme without the scheduler, which is analytically derived by the delay profile with $\tau_{RMS} = 200$[nsec], is shown in Fig. 10. From Fig. 10, it is seen that the uncoded BER performance with the proposed scheduler is better than that without the scheduler for $\Psi = 8$ and 16 in all the values of $\overline{E_s/N_0}$, and that the MC-CDM scheme without the scheduler provides better performance for $\Psi = 1$ in $\overline{E_s/N_0} > 6$, as opposed to the coded BER performance shown in Fig. 8. By comparing the uncoded BER performance in Fig. 10 with the coded BER performance in Fig. 8, it is considered that the MC-CDM scheme with the proposed scheduler could not make efficient diversity effects caused by the channel coding. This is because the transmission data of the user is spread in the single segment. On the other hand, the MC-CDM scheme without the scheduler can make efficient use of the frequency diversity effect caused by the channel coding, since the transmission data of the user is spread to all over the subcarriers.

When τ_{RMS} is varied in $\overline{E_s/N_0}$=6 [dB], Figs. 11 and 12 show the coded and uncoded BER performance of the MC-CDM scheme with and without the proposed scheduler for Ψ =1, 8 and 16, respectively. The uncoded and coded BER performance of the MC-CDM scheme with the proposed scheduler becomes better as the RMS delay spread, i.e., the frequency selectivity increases due to the multi-user diversity effect. That is, the delay spread increases as the variation in the frequency channel response is higher and the improvement of the frequency scheduling is also larger. On the other hand, the performance of the no-scheduled MC-CDM scheme is also better as the delay spread increases because of the frequency diversity effect. In common with Fig. 8, the coded BER performance of the proposed system is worse than that of the no-scheduled MC-CDM scheme for $\Psi = 16$ in $\tau_{RMS} > 200$. This is because the frequency diversity gain caused by the channel coding for the no-scheduled MC-CDM scheme is higher than the improvement from the multi-user diversity effect for the scheduled MC-CDM scheme in the case of τ_{RMS} >200 [nsec] and $\overline{E_s/N_0}$ =6 [dB].

Figure 13 shows the coded BER versus user number index ψ for the MC-CDM scheme with and without the proposed scheduler for $\Psi = 8$ and 16 in $\overline{E_s/N_0}$=2 [dB]. From the figure, we can recognize that the performance of the proposed system becomes better as the user number index ψ decreases, while that of the no-scheduled MC-CDM scheme is approximately flat for all the values of ψ. This is because the proposed scheduler can allocate the transmission segment with the higher SINR for the lower ψ th user. In other words, the proposed scheduler, which selects the user num-

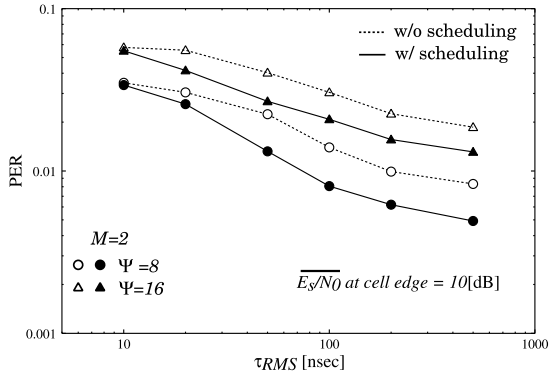

Fig. 14 PER versus τ_{RMS} for Ψ = 8 and 16. ($\overline{E_s/N_0}$ = 10 [dB] at cell edge)

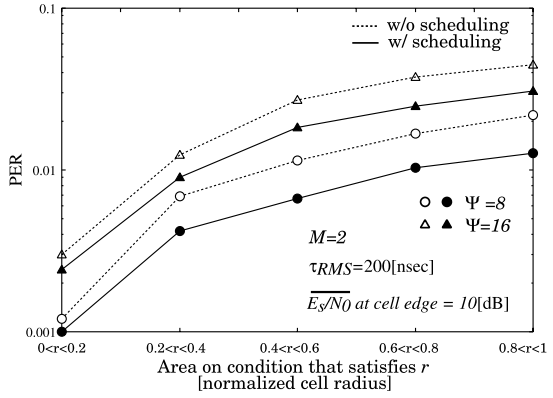

Fig. 15 PER versus *area* for Ψ = 8 and 16. (τ_{RMS} =200 [nsec] and $\overline{E_s/N_0}$ =10 [dB] at cell edge)

ber index ψ appropriately, can control the PER among the active users.

4.2 Multi-Cell Environment

In this subsection, the packet error rate (PER) performance of the proposed system with the channel coding is evaluated in the multi-cell environment. Here, the transmit signal power of the base station meets the requirement for $\overline{E_s/N_0}$ = 10 [dB] at the cell edge. For the sake of comparison, we also show the PER performance of the MC-CDM scheme without the proposed scheduler.

In the multi-cell environment where τ_{RMS} is varied, the PER performance of the MC-CDM scheme with and without the proposed scheduler is plotted in Fig. 14. The PER of the two schemes becomes smaller as the delay spread increases, and the performance of the MC-CDM scheme with the proposed scheduler is better than that without the scheduler for all the values of τ_{RMS}. As discussed in Sect. 4.1, the improvement is due to the fact that there is also a relationship between the delay spread and the diversity effects for the two schemes even in the multi-cell environment.

For τ_{RMS} =200 [nsec], Fig. 15 shows the PER performance per *area* for the distance of the user from the base station r (normalized by cell radius). Defining the number of erroneous packets and transmitted packets n_e and n_t, respectively, the PER for the *area* of $a < r < b$ is given by

$$PER_{a<r<b} = \left.\frac{n_e(r)}{n_t(r)}\right|_{a<r<b}. \quad (22)$$

The influence of interfering signals from the adjacent cells becomes larger as r increases. From Fig. 15, in the near center region the performance difference between the scheduling and the no-scheduling is small, while in the near outside region, the difference is large. This fact implies that the proposed scheduler, which autonomously and dynamically allocates the segment with higher SINR in own cell, can suppress the degradation due to the inter-cell interfering signals.

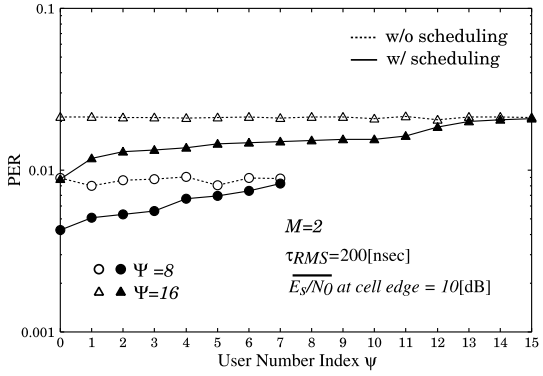

Fig. 16 PER versus user number index ψ for Ψ = 8 and 16. (τ_{RMS} =200 [nsec] and $\overline{E_s/N_0}$ =10 [dB] at cell edge)

For τ_{RMS} =200 [nsec], Fig. 16 shows the PER user number index ψ for the MC-CDM scheme with and without the proposed scheduler for Ψ = 8 and 16. As is the case with the single-cell environment, we can recognize that the performance of the proposed system becomes better as the user number index ψ decreases, while that of the no-scheduled MC-CDM scheme is flat for all the values of ψ. Therefore, the proposed system can control the QoS in terms of the PER among the users even in the multi-cell environment.

5. Conclusion

In this paper, we have proposed a frequency scheduling method for an MC-CDM scheme. The performance of the proposed system has been evaluated by computer simulation in both single- and multi-cell environments. Computer simulation results have shown that

- Due to the multi-user diversity effects, the proposed system can facilitate allocation of the segment with higher SINR than average SINR in all the received subcarriers for the no-scheduled MC-CDM scheme.
- The proposed system mitigates the inter-cell interfering signals in the multi-cell environment.
- Selecting the user number among active users, the proposed system can control the QoS among the active users.

Consequently, the proposed system is suitable for the MC-CDM scheme to achieve the high-rate data transmission in the multi-cell environment.

Our future work includes applying the proposed scheduling method to an MC-CDM scheme with combination of time and frequency spreadings [22], [23] in order to more improve its performance. In the system, the configuration of segment including time and frequency domains can be more flexible due to the time and frequency spreadings, and it affects the scheduling performance. Therefore, analyses introducing the configuration with various system parameter settings are required in our further work. Moreover, the performance of the proposed scheduling method is studied for practical environments. For example, the SINR information for the segment available at the base station does not always correspond with its true value due to the channel estimation error and the time-selectivity of the channel. Our future work includes these challenging issues.

References

[1] S. Hara and R. Prasad, "Overview of multicarrier CDMA," IEEE Commun. Mag., vol.35, no.12, pp.126–133, Dec. 1997.
[2] S. Abeta, H. Atarashi, M. Sawahashi, and F. Adachi, "Performance of coherent multi-carrier/DS-CDMA and MC-CDMA for broadband packet wireless access," IEICE Trans. Commun., vol.E84-B, no.3, pp.406–413, March 2001.
[3] S. Hara and R. Prasad, "Design and performance of multi-carrier CDMA system in frequency selective fading channel," IEEE Trans. Veh. Technol., vol.48, no.5, pp.1584–1595, Sept. 1999.
[4] H. Atarashi, S. Abeta, and M. Sawahashi, "Comparison of broadband packet wireless access," IEICE Technical Report, RCS2000-136, Oct. 2000.
[5] S. Abeta, H. Atarashi, and M. Sawahashi, "Performance comparisons of broadband packet wireless access schemes for forwardlink high-speed transmission in multi-cell environment," IEICE Technical Report, RCS2000-50, June 2000.
[6] 3GPP, TR25.848, "Physical layer aspects of UTRA high speed downlink packet access," Release 4, 2001.
[7] R.A. Jalali and R. Pankaj, "Data throughput of CDMA-HDR a high efficiency-high data rate personal communication wireless system," IEEE VTC2000 Spring, Tokyo, Japan, May 2000.
[8] W. Rhee and J. Cioffi, "Increase in capacity of multiuser OFDM system using dynamic subchannel allocation," IEEE VTC 2000 Spring, pp.1085–1089, Tokyo, May 2000.
[9] V. Lau, "Proportional fair scheduling for wireless access point with multiple antenna-reverse link with scalar feedback," IEEE GLOBECOM 2002, pp.763–767, Taipei, Taiwan, ROC, Nov. 2002.
[10] B. Classon, P. Sartori, V. Nangia, X. Zhuang, and K. Baum, "Multi-dimensional adaptation and multi-user scheduling techniques for wireless OFDM systems," IEEE ICC 2003, pp.2251–2255, Anchorage, AK, May 2003.
[11] M. Ergen, S. Coleri, and P. Varaiya, "QoS aware adaptive resource allocation techniques for fair scheduling in OFDMA based broadband wireless access systems," IEEE Trans. Broadcast., vol.49, no.4, pp.362–370, Dec. 2003.
[12] M. Ura, Y. Hara, and Y. Kamio, "Segment allocation algorithm for multimedia MC-CDMA," IEICE Technical Report, RCS2000-261, March 2000.
[13] Y. Hara, T. Kawabata, J. Duan, and T. Sekiguchi, "MC-CDM system for packet communications using frequency scheduling," IEICE Technical Report RCS2002-130, July 2002.
[14] S. Tsumura and S. Hara, "A frequency scheduling method using antenna diversity for MC-CDM system," IEEE VTC2003-Spring, pp.1253–1257, Jeju, Korea, April 2003.
[15] C. Berrou, A. Glavieux, and P. Thitimajshima, "Near Shannon limit error-correcting coding and decoding: Turbo-codes(1)," IEEE International Communications Conference, pp.1064–1070, Geneva, Switzerland, May 1993.
[16] E. Dinan and B. Jabbari, "Spreading codes for direct sequence CDMA and wideband CDMA cellular networks," IEEE Commun. Mag., vol.36, no.9, pp.48–54, Sept. 1998.
[17] S. Hara, S. Tsumura, and Y. Hara, "Performance analysis of MC-CDM and cyclically prefixed DS-CDM," IEICE Technical Report, WBS2003-153, March 2004.
[18] S. Hara, Y. Hara, and S. Tsumura, "Analysis of MC-CDM and cyclically prefixed DS-CDM," IEEE PIMRC 2004, Sept. 2004 (in CD-ROM).
[19] D. Reynolds and X. Wang, "Low complexity turbo-equalization for diversity channels," Signal Process., vol.81, no.5, pp.989–995, May 2001.
[20] S. Tsumura, M. Vehkaperä, Z. Li, D. Tujkovic, M. Juntti, and S. Hara, "Performance evaluation of turbo and space-time turbo coded MC-CDMA downlink in single and multi-cell environments," IEICE Trans. Commun., vol.E87-B, no.10, pp.3011–3020, Oct. 2004.
[21] A. Chouly, A. Brajal, and S. Jourdan, "Orthogonal multicarrier techniques applied to direct spread spectrum CDMA systems," IEEE GLOBECOM 1993, pp.1723–1728, Nov. 1993.
[22] A. Sumasu, T. Nihei, K. Kitagawa, M. Uesugi, and O. Kato, "An OFDM-CDMA system using combination of time and frequency domain spreading," IEICE Technical Report, RCS2000-3, April 2000.
[23] A. Persson, T. Ottosson, and E. Storöm, "Time-frequency localized CDMA for downlink multi-carrier system," IEEE ISSSTA 2002, pp.118–122, Prague, Czech Republic, Sept. 2002.

Shigehiko Tsumura received the B.Eng. and M.Eng. degrees in communication engineering from Osaka University, Osaka, Japan, in 2000 and 2002, respectively. He is currently a Ph.D. candidate at graduate school of engineering, Osaka University. His research interests include wireless communications systems and digital signal processing. He is a Student Member of IEEE.

Yoshitaka Hara received the B. E., M. E., and Dr.Eng. degrees from the University of Tokyo, Tokyo, Japan, in 1993, 1995, and 2003, respectively. In 1996, he joined Mitsubishi Electric Corporation. From 1999 to 2001, he was also a senior research engineer at YRP Mobile Telecommunications Key Technology Research Laboratories Co., Ltd. Since 2003, he has been with the Mitsubishi Electric Information Technology Centre Europe B.V. (ITE). His research interests include CDMA sytems and adaptive antenna arrays.

Shinsuke Hara received the B.Eng., M.Eng. and Ph.D. degrees in communication engineering from Osaka University, Osaka, Japan, in 1985, 1987 and 1990, respectively. Now, he is an Associate Professor in the Department of Electronic, Information Systems and Energy Engineering, Graduate School of Engineering, Osaka University. From April 1996 to March, he was a Visiting Scientist in Telecommunications and Traffic Control Systems Group, Delft University of Technology, Delft, The Netherlands. His research interests include satellite, mobile and indoor wireless communications systems, and digital signal processing. Dr. Hara is a Member of IEEE.